Efficient Inverse Modeling Framework for Energy Transition Applications Using Operator-Based Linearization and Adjoint Gradients

Tian, Xiaoming; Voskov, Denis

DOI
10.2118/212169-MS

Publication date
2023

Document Version
Final published version

Published in
SPE Reservoir Simulation Conference 2023 Proceedings Papers

SPE-212169-MS

Efficient Inverse Modeling Framework for Energy Transition Applications Using Operator-Based Linearization and Adjoint Gradients

Xiaoming Tian, TU Delft, Denis Voskov, and TU Delft, Stanford University

 DOI 10.2118/212169-MS

This paper was prepared for presentation at the SPE Reservoir Simulation Conference held in Galveston, Texas, USA, 28–30 March 2023.

Abstract

In this paper, we present an efficient inverse modeling framework for energy transition applications. The key feature of this framework is a combination of adjoint gradients and Operator-based Linearization (OBL) technique to achieve high efficiency in inverse modeling based on forward simulations. This framework allows conducting the history matching of practical industrial applications using the gradient descent method with considerable model control variables in a reasonable time. Generally, the inverse modeling of industrial applications involves large amounts of gradient calculations in algorithms based on gradient descent. In this study, we analytically compute the gradient using the adjoint gradient method as an alternative to the widely used numerical gradient method where many time-consuming forward simulation runs are needed. In the adjoint gradient approach, the objective function is linearly combined with the governing equation by introducing a Lagrange multiplier. That allows for finding the analytical gradient in a backward manner. The developed adjoint gradient method takes full advantage of the OBL efficiency and flexibility when assembling the Jacobian and some relevant derivatives. We demonstrate the applications of the proposed inverse modeling framework to different energy transition applications, including petroleum production, extraction of geothermal energy, and CO_2 storage. We demonstrate various treatments of objective function definitions, well controls, and measurement errors for these industrial applications. For petroleum production, the proposed framework is tested on the multiphase multi-component flow problem, which is illustrated by an example of data-driven Discrete Well Affinity model. For this application, only production data is considered. The geothermal problem involves an additional energy balance equation and various property calculations for water and steam. In this application, together with the production data, additional electromagnetic monitoring is used in the history matching process. The results show that electromagnetic monitoring significantly improves the inversion process. We conclude the description of our framework with an application relevant to CO_2 sequestration process. The CO_2 storage modeling is complicated due to the complex physical phenomena to be considered. In this application, tracer data are used as an additional observation, which allows considering uncertainties in the dynamics of CO_2. In this study, the adjoint gradient method is specially designed and customized for OBL infrastructure of the Delft Advanced Research Terra Simulator (DARTS). This allows us to design the general-purpose inversion module with efficient gradient computation, while most existing simulation platforms lack this

capability. Based on the multiphysics simulation engine in DARTS, the various observation information can be combined in the proposed framework. This allows us to solve the general-purpose inverse modeling problems for most energy transition applications.

Introduction

With the increasing amounts of carbon emission and atmospheric pollution due to the burning of fossil fuels, more and more governments and institutes started to initiate and conduct various energy transition policies. Those policies include (but are not limited to): improving energy efficiency and promoting energy conservation; using the low carbon fuels; developing renewable energy; afforestation and reforestation; and CO_2 capture and storage (Leung et al., 2014). Amongst these approaches and policies, there are some techniques that are related to underground fluid flows, for example, geothermal energy, CO_2 storage, natural gas, hydrogen storage, etc.

Numerical simulation is a powerful tool to help engineers and industries to analyze the evaluate the feasibility of those underground energy transition projects. However, the complexity of the geological model and the calculation of physical properties cause difficulties in solving linearized systems. The upscaling method mainly focuses on reducing the complexity of the geological model to achieve better performance by utilizing a coarse grid to replicate the high-fidelity model response (Durlofsky, 2005). Multi-scale method (Hou and Wu, 1997; Jenny et al., 2003) and streamline simulation (Datta-Gupta and Datta-Gupta, 2007) share the similar idea of reducing the degrees of freedom of the reservoir model to compute the model response without losing much accuracy.

An alternative approach is to reduce the computational cost of the calculation of physical properties, for example, the flash calculation. The Compositional Space Parametrization (CSP) for compositional simulation was proposed to improve the nonlinear convergence and therefore reduce the cost in iterations (Zaydullin et al., 2012, 2013). Later, Voskov (2017a) proposed Operator-Based Linearization (OBL) approach to "pre-process" the calculation of the physical properties and their associated derivatives. This approach reduces large amount of calculations of physical properties in the course of Jacobian assembly. Instead, it only calculates the properties at certain fixed supporting points. For those physical properties lying in the area formed by the supporting points, they are efficiently interpolated from the values at the supporting points. This approach was further improved by introducing the adaptive parameterization of the physical parameter space (Khait and Voskov, 2018a). This OBL approach was incorporated into the reservoir simulation framework Delft Advanced Research Terra Simulator (DARTS).

With the development of various advanced open-source reservoir simulation frameworks, many of them are applied to simulate the physical process of energy transition projects. Lie et al. (2015) utilized the framework of MATLAB Reservoir Simulation Toolbox (MRST) to simulate the CO_2 storage process and proposed a simulation workflow for the large-scale CO_2 storage project. Voskov et al. (2017) modeled various CO_2 sequestration mechanisms based on fully compositional multi-scale simulation using a combination of reservoir simulator (ADGPRS) and chemical solver (GFLASH). Similar developments have been performed in DuMux with a focus on early timescale chemical reactions relevant to CO_2 sequestration Ahusborde et al. (2021). Lyu et al. (2021) investigated foam-assisted CO2 storage in saline aquifers using the reservoir simulation framework Delft Advanced Research Terra Simulator (DARTS). Khait and Voskov (2018c) and Wang et al. (2020) utilized DARTS for the application of geothermal reservoir simulation. Kong et al. (2017) simulated and conducted the optimization of the well placement of the geothermal doublets system based on the simulator OpenGeoSys.

All of the aforementioned examples are about the utilization of forward simulation of energy transition applications assuming certain model parameters. However, it is crucial to inverse and calibrate the model before conducting the numerical simulation in order to match the historical data from the field. Guo et al. (2018) proposed a data-driven history matching named Interwell Numerical Simulation Model with Front-

Tracking (INSIM-FT). However, the model used in the INSIM-FT method is highly simplified into several reservoir nodes and well nodes. Although more nodes can be introduced, this increases the computational cost for the evaluation of gradient in the history matching iterations. Tian et al. (2021) introduced a data-driven Discrete Well Affinity (DiWA) model. Instead of using a highly simplified reservoir model, a coarse model that contains the basic geological information (e.g. the contour, thickness, etc.) is taken as the basis to train the model. At the same time, the adjoint method is implemented in the DiWA framework to increase the efficiency of the gradient evaluation. The DiWA method was later extended to the stochastic DiWA method (Tian and Voskov, 2022). To quantify the uncertainty of the model, the method of Randomized Maximum Likelihood and Maximum A-Posteriori were also introduced in the inverse modeling of reservoir simulation (Stordal and Nævdal, 2017; Bukshtynov et al., 2015; Vo and Durlofsky, 2014; Evensen et al., 2022).

This study will focus on inverse modeling for energy transition applications. First, the governing equations of the energy transition applications are demonstrated and the OBL method is implemented to linearize the governing equation system. The inverse modeling framework is then explained based on the introduction of the objective function and the adjoint method. With the proposed inverse modeling framework, we conducted the history matching to a real hydrocarbon production reservoir, a geothermal reservoir, and an experimental CCS project to test the performance of this framework. Various types of misfits are considered in the objective function, including well rates, BHP, well temperature, and time-lapse reservoir data. The results show that the computational time of training of both geothermal and CCS tracer test model can be finished within hours, even though the number of control variables is more than 70000 in each model. The model responses have a good match with the observations of well rates and time-lapse data. The permeability result also shows that the optimizer is able to capture the characteristics of the fluid flow pattern, especially in the region of plumes where the fluid dynamics are very pronounced.

Forward simulation

The energy transition simulation problem involves solving the energy and mass governing equations. In this section, the governing equation coupling both energy and mass terms are described. Their discretization and linearization based on the operator forms are introduced and discussed.

Governing equations

The energy and mass conservation equations describe a flow dynamic system bounded in the domain with volume Ω and surface Γ. The conservation equation can be written as:

$$\frac{\partial}{\partial t}\int_{\Omega} M^c d\Omega + \int_{\Gamma} \boldsymbol{F}^c \cdot \boldsymbol{n} d\Gamma = \int_{\Omega} Q^c d\Omega, \tag{1}$$

where M^c is the accumulation term for the c^{th} component ($c = 1,\ldots, n_c$, index of the mass components [e.g., water, CO_2] and $c = n_c + 1$, index of the energy quantity); $\boldsymbol{F}_c$ is the flux term of the c^{th} component; $\boldsymbol{n}$ is the unit normal direction pointing outward to the domain boundary; Q_c is the source/sink term of the c^{th} component. The detailed explanations of M^c, $\boldsymbol{F}_c$, and Q_c can be found in Wapperom et al. (2022).

To solve this mass and energy conservation equation numerically, it needs to be discretized spatially and temporally. Based on the finite volume method using two-point flux approximation, the discretized form of Equation (1) for the i^{th} reservoir gridblock can be written as:

$$g_i^c = V_i\left(M_i^c(\omega_i) - M_i^c(\omega_{i(k-1)})\right) - \Delta t\left(\sum_l a_l F_l^c(\omega) + V_i Q_i^c(\omega)\right) = 0, \quad c = 1, \ldots, n_c + 1. \tag{2}$$

Equation (2) shows the residual form of discretized Equation (1). V_i is the volume of the i^{th} gridblock. ω_i is the state variables at the current time step. $\omega_{i(k-1)}$ is the state variables at previous time step. Δt is the time step. a_l is the contact area of the interface l between neighboring grids.

The operator-based linearization (OBL) approach (Voskov, 2017b) is employed in DARTS to linearize the governing equation of Equation (1). The main idea of OBL is discretizing the physical space to improve the efficiency of various physical property calculations. This approach was proposed and validated for complex multi-phase flow problems coupled with the thermal process. With the OBL method, the governing equation is written in form of state-dependent operators. The values and derivatives of the operators can be evaluated and interpolated based on supporting points under the different resolutions of physical parameter space. A more advanced adaptive parameterization technique for OBL calculation was further proposed to largely reduce the computational time of parameterization in high-dimension physical parameter space (Khait and Voskov, 2018b). Compared with the conventional Jacobian assembly procedure in numerical simulation, the OBL method makes the Jacobian assembly procedure more flexible and efficient for highly complex physical problems. More details about the OBL can be found in Voskov (2017b), Khait and Voskov (2017), and (Khait and Voskov, 2018b).

Well treatment

The well controls and constraints are inner boundary conditions of the governing equations. In DARTS, a connection-based multi-segment well model is used to simulate the flow in the wellbore (Khait and Voskov, 2019). Multiple well blocks representing the perforations are connected to the reservoir girdblocks. Those well blocks (i.e. well body) are then connected to a ghost well block (i.e. well head). This ghost well block is actually the placeholder where the well controls and constraints are added.

For bottom hole pressure (BHP), a target pressure value is defined at the ghost well block:

$$p - p^{target} = 0. \tag{3}$$

The volumetric rate control is implemented through the volumetric rate operator ζ_j^{vol}:

$$T^s \zeta_j^{vol}(\omega) \Delta p - Q^{target} = 0, \tag{4}$$

where

$$\zeta_j^{vol} = \frac{\hat{s}_j(\omega) \sum_c \beta_{cj}(\omega)}{\hat{\rho}_t(\omega)}; \tag{5}$$

Q^{target} is the target volumetric flow rate at separator conditions [m^3/day]; $\hat{s}_j$ and $\hat{\rho}_j$ are the saturation and total fluid density respectively at separator conditions; T^s is the well segment transmissibility between well head and well body; $\beta_{cj}(\omega)$ is the mass flux operator:

$$\beta_{cj}(\omega) = x_{cj} \rho_j k_{rj} / \mu_j, c = 1, \ldots, n_c, \; j = 1, \ldots, n_p. \tag{6}$$

x_{cj} is molar fraction of c component in j phase. ρ_j, k_{rj}, and μ_j are the density, relative permeability, and viscosity of phase j, respectively. In the thermal model, the BHP and volumetric rate control can be coupled with the thermal well control. Specifically, the temperature well control in DARTS is written as:

$$\chi(\omega) - T^{\text{target}} = 0, \tag{7}$$

where T^{target} is the target temperature of injected fluid, $\chi(\omega)$ is dependent on the thermodynamic state ω.

Inverse modeling

Instead of conducting inverse modeling with the conventional numerical gradient-based method, the adjoint method is applied in this study to increase the gradient calculation efficiency. In this section, we will introduce the general form of the adjoint method.

The derivations shown in this section will mostly follow the notation of Jansen (2011) and Volkov and Voskov (2016). The main idea of the adjoint method is that the original objective function J is linearly combined with the governing equations g (i.e. Equation (2)) to construct an augmented objective function $\overline{J}$:

$$\overline{J}(\omega, u, \lambda) = J(\omega, u) + \lambda^{T} g(\omega, u). \tag{8}$$

A transposed form of Lagrange multiplier λ^{T} is introduced in the augmented objective function. J is the original objective function. u is the control variable of the inverse modeling problem. In this study, the transmissibility and well index are taken as the control variables in the inverse modeling problem. The extrema of Equation (8) are located either at the boundary of the feasibility region or at stationary points. Here we will not discuss about the case that the extrema are located at the feasibility region boundary, because this is a relatively simple situation. For the case of stationary points, all first-order derivatives with respect to all variables λ, ω, and u should be equal to zero. This leads to the following equations:

$$\overline{J}_{\lambda} = g(\omega, u) = 0, \tag{9}$$

$$\overline{J}_{\omega} = \lambda^{T} g\omega(\omega, u) + J_{\omega}(\omega, u) = 0, \tag{10}$$

$$\overline{J}_{u} = \lambda^{T} g_{u}(\omega, u) + J_{u}(\omega, u) = 0. \tag{11}$$

The Equation (9), Equation (10), and Equation (11) shows the first-order derivatives of the augmented objective function $\overline{J}$ with respect to λ, ω and u, respectively.

Apparently, Equation (11) is our main focus to be solved. Because $\overline{J}_{u}$ is the gradient with respect to the control variables u. In the inverse modeling, the optimizer will use the gradient $\overline{J}_{u}$ to search for the optimum in the control variable space. To compute $\overline{J}_{u}$, apart from the computation of the derivatives $g_u(\omega, u)$ and $J_u(\omega, u)$, the Lagrange multiplier λ^{T} needs to be solved from Equation (10). As for the Equation (9), it is actually the residual form of governing equation (i.e. Equation (2)) and already satisfied in forward simulation.

In the numerical simulation, the governing equations are discretized both spatially and temporally. To implement the adjoint method, Equation (9), Equation (10), and Equation (11) should also be reformed into discretized formulation correspondingly. Denote the discretized governing equation at k^{th} time step as:

$$g_{k}(\omega, \omega_{(k-1)}, u) = 0, \tag{12}$$

where $\omega_{(k-1)}$ represents the state variables at previous time step. The discretized objective equation J reads:

$$J = \sum_{k=1}^{k} L_{k}, \tag{13}$$

where K is the total number of the simulation time steps, L_k is the misfit between the model response and the observation data at the given simulation time step k. The misfit term L_k is defined as:

$$L_{k} = (f_{1} + f_{2} + f_{3} + f_{4})\delta_{t}(\tau_{0bs}), \tag{14}$$

where $\delta_t(\tau_{obs})$ is Dirac measure function and is given as:

$$\delta_{t}(\tau_{obs}) = \begin{cases} 1 & \text{if} \quad t \in \tau_{obs} \\ 0 & \text{if} \quad t \notin \tau_{obs} \end{cases}, \tag{15}$$

where t is the time point at the endpoint of a given simulation time interval, τobs is a set of the observation time points, which means it is a subset of the simulation time points. As for the expressions of f_1, f_2, f_3, and f_4, their expressions are:

$$
\begin{aligned}
f_1 &= \sum_{w=1}^{\mathrm{nw}} \sum_{j=1}^{\mathrm{np}} C_{w,j}^{rate}\left(q_{w,j} - q_{w,j}^{*}\right)^2 \\
f_2 &= \sum_{w=1}^{\mathrm{nw}} C_{w}^{BHP}\left(T_w - p_w^{*}\right)^2 \\
f_3 &= \sum_{w=1}^{\mathrm{nw}} C_{w}^{Twell}\left(T_w = T_w^{*}\right)^2 \\
f_4 &= \sum_{m=1}^{\mathrm{nblock}} C_{m}^{Tres}\left(\Theta_m - \Theta_m^{*}\right)^2,
\end{aligned}
\tag{16}
$$

where f_1, f_2, and f_3 are the terms representing the misfit between the model response and the observation data monitored at the wells. They are well phase flow rate, well bottom hole pressure (BHP), and well temperature, respectively. The term f_4 designates the misfit between the model response of the reservoir block time-lapse data and the effective reservoir block time-lapse observations interpreted from the geophysical data, for example, the electromagnetic (EM) data or seismic data (Bukshtynov et al., 2015). Here, n_w, n_p, and n_{block} are the number of wells, phases, and reservoir blocks, respectively. $q_{w,j}$ is the model response of the rate of well w and phases j. p_w is the BHP of the well w. T_w is the temperature of well w. Θ_m is the effective time-lapse data of reservoir block m. The superscript * denotes the corresponding observation data of the terms in Equation (16). The notation C with the corresponding subscripts and superscripts defines the inverse of the diagonal covariance matrices of measurement errors.

Now, with the discretized g_k and L_k prepared, the discretized form of Equation (10) can be written as:

$$
\lambda_{k+1}^{\mathrm{T}} \frac{\partial g_{k+1}}{\partial \omega_k} + \lambda_k^{\mathrm{T}} \frac{\partial g_k}{\partial \omega_k} + \frac{\partial L_k}{\partial \omega_k} = 0, \tag{17}
$$

$$
\lambda_{\mathrm{K}}^{\mathrm{T}} \frac{\partial g_{\mathrm{K}}}{\partial \omega_{\mathrm{K}}} + \frac{\partial L_{\mathrm{K}}}{\partial \omega_{\mathrm{K}}} = 0. \tag{18}
$$

The discretized form of Equation (11) reads:

$$
\bar{g}_u = \sum_{k=1}^{\mathrm{K}} \left(\lambda_k^{\mathrm{T}} \frac{\partial g_k}{\partial u_k} + \frac{\partial L_k}{\partial u_k} \right). \tag{19}
$$

Equation (19) will be utilized in the gradient-based algorithm in history matching.

Energy transition applications

In this section, we will provide three examples of energy transition applications including optimal hydrocarbon production, geothermal energy and CO_2 storage project. These three models utilize different types of mesh to represent the geological structures of interest. All examples include the history matching to different types of dynamic data.

The application of Discrete Well Affinity (DiWA) model

Here we present an application of the data-driven DiWA model to provide a forecast for a real hydrocarbon production reservoir. Data-driven proxy models based on physics are getting quite popular since they often are based on consistent physical concepts which help to provide an accurate model response after appropriate training procedures. DiWA model proves its efficiency in the production forecast for synthetic problems Tian et al. (2021); Tian and Voskov (2022). In this example, we show how useful DiWA model can be for the production forecast and data diagnostic for the real reservoir.

The DiWA model is based on the approximate representation of the reservoir in question using a coarse unstructured grid which approximates the affinity of wells. In this model, three types of parameters are

usually used as the control variables for data assimilation: transmissibility, well indices, and rock-fluid interaction parameters. The prior distribution of the control variables is sampled from the standard statistics of the reservoir based on the measured data such as the interpretation of logs, cores, and analog models. Based on sampled parameters, the initial filtering is applied using the misfit between the true production data and the DiWA model response. Filtered models generate a prior ensemble for the following history-matching procedure.

Based on the prior ensemble, we perform a history matching using Maximum Likelihood Estimation (MLE) with numerical derivatives for rock-fluid interaction control variables and adjoint gradients for transmissibilities and well indices. The results of the raw DiWA model application are used then for data diagnostic. In Figure 1, we show one problematic well with an obvious deviation from historic observations. You can notice a lower water production in the initial production and an extreme water rate peak in the depletion period. Further investigation showed that this well was completed in two pay zones which have never been reflected in the proxy model. Later, the work-over operation on this well leads to a significant water peak which has no relation to the reservoir dynamic but creates a significant mismatch in the model training.

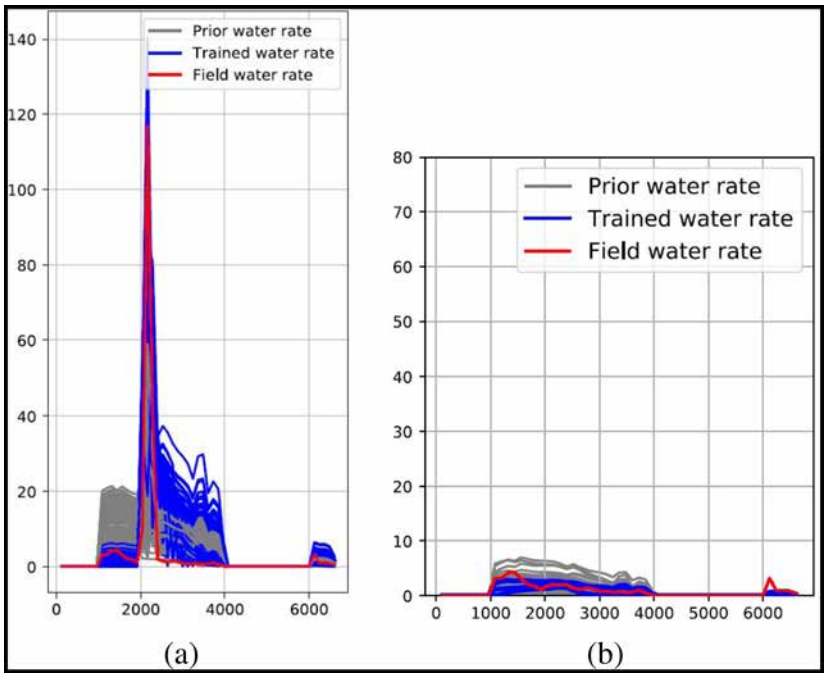

Figure 1—The diagnostic and the associated correction of problematic well using DiWA model. Figure (a) and (b) are the history matching results of this well before and after the correction of the water rate peak, respectively

After several adjustments to the conceptual DiWA model based on the data diagnostic study, we applied a second attempt for the history matching using the same MLE approach. In the second attempt of history matching, we are going to include both the depletion and waterflooding periods. After applying consistent adjustments like filtering, re-scaling by different weights, and revising boundary conditions in the course of data quality diagnostics, the final results are shown in Figure 2.

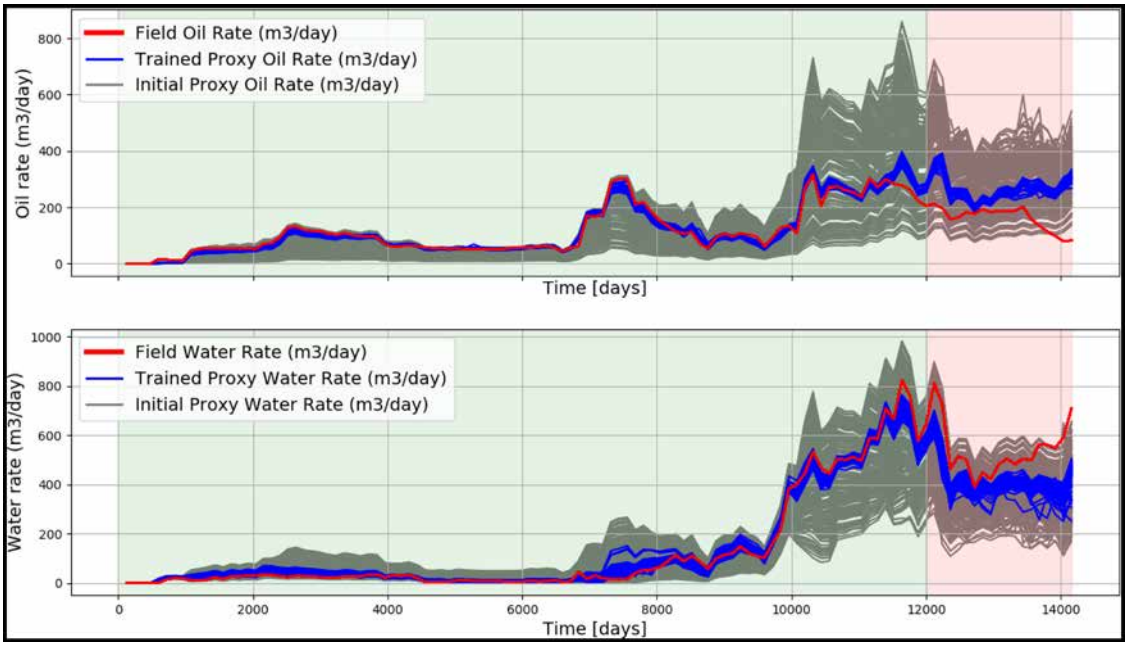

Figure 2—The final history matching results of the total oil and water rates of both depletion and flooding periods

The application of geothermal project

The geothermal reservoir simulation involves the process of thermal transfer in the porous media. Heat transfer mainly includes two physical processes: heat conduction and heat convection. The geothermal doublet well is widely used for geothermal energy extraction. Typically, the geothermal water is produced from the producer and the same amount of water is re-injected into the reservoir through the injector. Since the doublet geothermal system is dominated by heat convection, the transmissibility will be taken as the main control variable in this study in the inverse modeling.

The Egg model is a three-dimensional channelized reservoir model with a structured mesh grid. It is an open-access model ensemble containing 100 permeability realizations (Jansen et al., 2014). The dimensions of the Egg model are 60 × 60 × 7 blocks with the block size of 30m × 30m × 12m. The permeability in the x direction is the same as that in y direction. They are imported from the dataset of the Egg model ensemble. The permeability in z direction is 0.1 times the permeability in x direction. The porosity of the reservoir is 0.2. The initial reservoir pressure and temperature are 200bar and 348.15K, respectively. The volumetric heat capacity of rock is 2200kJ/m^3/K. The thermal conductivity of rock is 181.44kJ/m/day/K. The direction of the doublet is almost perpendicular to the fluvial channels in the Egg model in order to prolong the production time before the cold breakthrough, see Figure 3. In this figure, the realization "PERM1_ECL.INC" is taken as an example to show the channelizedpattern in the Egg model. This realization will be utilized to generate the synthetic observations for history matching problem.

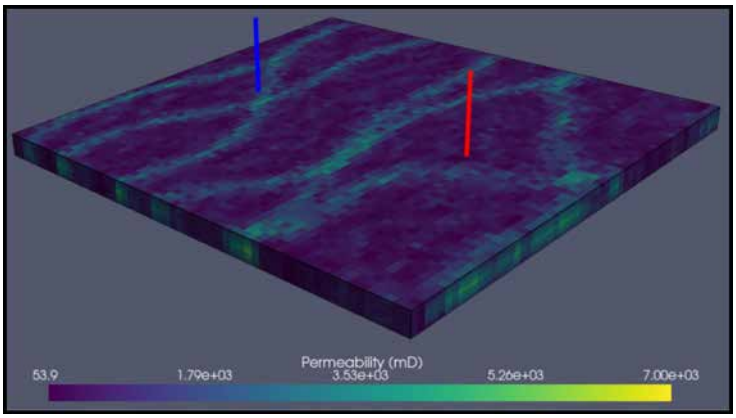

Figure 3—The permeability distribution of the realization "PERM1_ECL.INC". Multiple fluvial channels are distributed in this realization. The blue and red bars represent the location of the injector and producer, respectively

In this model, all seven layers are perforated for both the injector and producer. To "match" the production history and the time-lapse temperature data at the reservoir, 71174 control variables are iterated and updated simultaneously in the history matching procedure. These control variables include 71160 transmissibility for each block interface and 14 well indexes for each perforation of two wells. The "true" model "PERM1_ECL.INC" runs for 40 years in total. The data from the first 30 years are the observations for history matching. The data of the rest 10 years are utilized to check the performance of the forecast of the proposed inverse modeling framework.

Figure 4 shows the results of the temperature of production well. It can be seen that most trained realizations (the blue curves) fit the observations (the red curve) very well in the training period (the green area). In the forecasting period (the white area), the trained realizations have a wider range of well temperature profiles. Considering that most of the realizations have an absolute error smaller than 2 degrees in the forecasting period, this result is acceptable for the geothermal history matching problem.

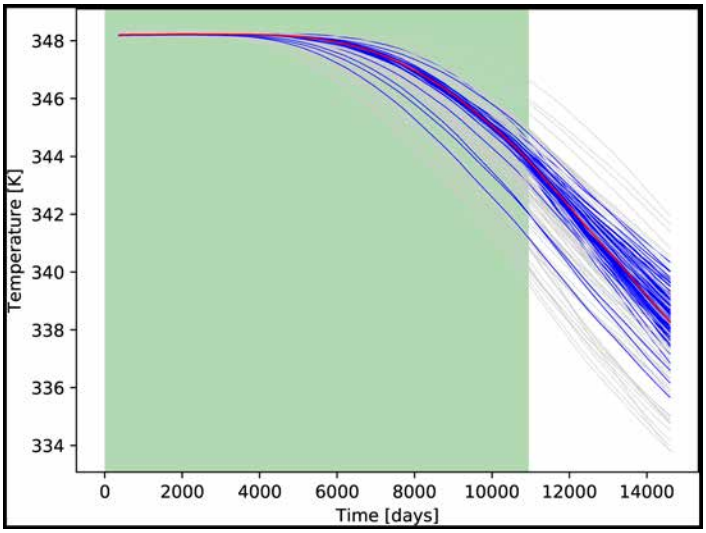

Figure 4—The history matching results of the temperature of the production well. The red curve is the observation data. The gray and blue curves are the results before and after history matching, respectively. The training period is located in the green area.

The realization "PERM61_ECL.INC" is taken as an example to demonstrate the results of the reservoir temperature and the permeability distribution. Figure 5 and Figure 6 are the results of the 4th layer of the realizations. As it can be seen from Figure 5, the reservoir temperature after the history matching is very similar to the EM data observation. This is because the optimizer has the tendency to block the

fluvial channels of the initial guess, and then re-construct the true permeability field, see the "permeability difference" in Figure 6. The "permeability difference" also reflects the accuracy of the adjoint gradient, as it is able to capture the characteristics of the permeability field and re-construct such intricate patterns of fluvial channels.

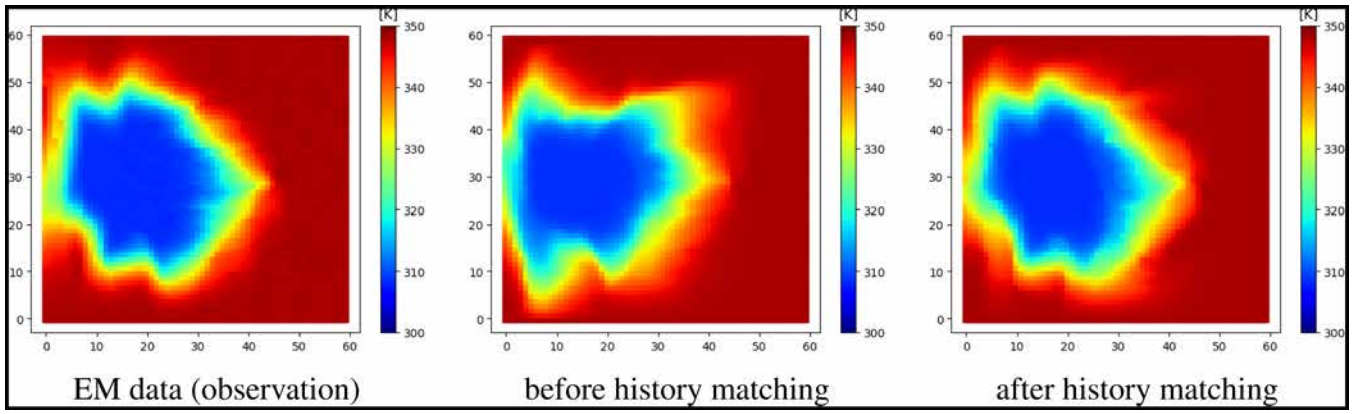

Figure 5—The reservoir temperature of the 4th layer of the realization "PERM61-ECL.INC". The left figure shows the EM observation data of the "true" model. The middle and right figures are the results before and after history matching.

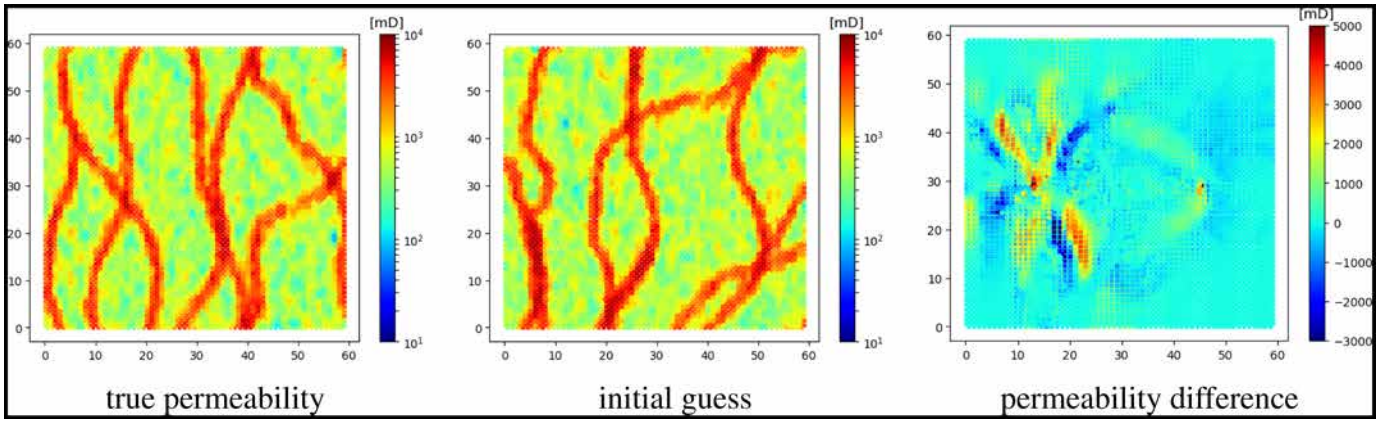

Figure 6—The permeability distribution of the 4th layer of the Egg model. The left figure shows the "true" permeability distribution of the realization "PERM1_ECL.INC" in the logarithmic scale. The middle figure is the initial guess (i.e. the realization "PERM61_ECL.INC"). The right figure demonstrates the difference of the permeability of "PERM61_ECL.INC" before and after history matching.

The computational time of training each realization is around 8 hours executing on the machine with the processor of 2x Intel XEON E5-6248R 24C 3.0GHz. Note that the adjoint gradient evaluation of 71174 control variables takes less than 400 seconds, while the computational time of a single forward simulation is around 15 seconds. Compared with the conventional numerical gradient evaluation, the adjoint gradient evaluation proposed in this framework is much more efficient especially when the dimension of the model is very large. For training the whole ensemble of realizations (i.e. 99 realizations except for "PERM1_ECL.INC"), we parallelly trained all realizations on DelftBlue cluster (Delft Blue, 2022) with multiple nodes and cores with the same processors mentioned above.

The application of CO_2 storage project

It is challenging work to simulate CO_2 storage numerically because of the complexity of the model physics. In this section, we will develop a numerical model of CO_2 storage FluidFlower project and conduct the history matching to the experimental tracer test of this project. The experimental time-lapse observations of the tracer will be fitted in the course of the history matching iterations.

An experimental rig was built to mimic the geological layering and the CO2 injection and storage process. Nine types of sand are filled into the rig to form multiple layers and three faults. Two injection wells are placed at the bottom left and the middle of the rig, see the red circle in Figure 7. The tracer was injected through the injection well at the rate of 2250 ml/h for 30 minutes and then 0 ml/h for 30 minutes. By repeating this procedure (including three time steps) three times, we get the experimental images of tracer plumes shown in Figure 8.

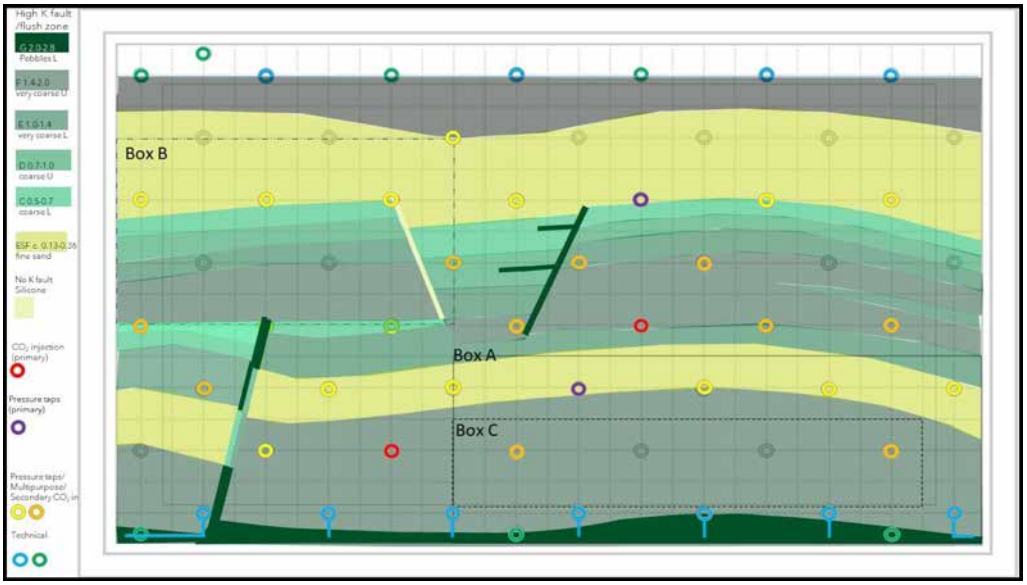

Figure 7—The sketch of the experimental rig geometry following FluidFlower benchmark description

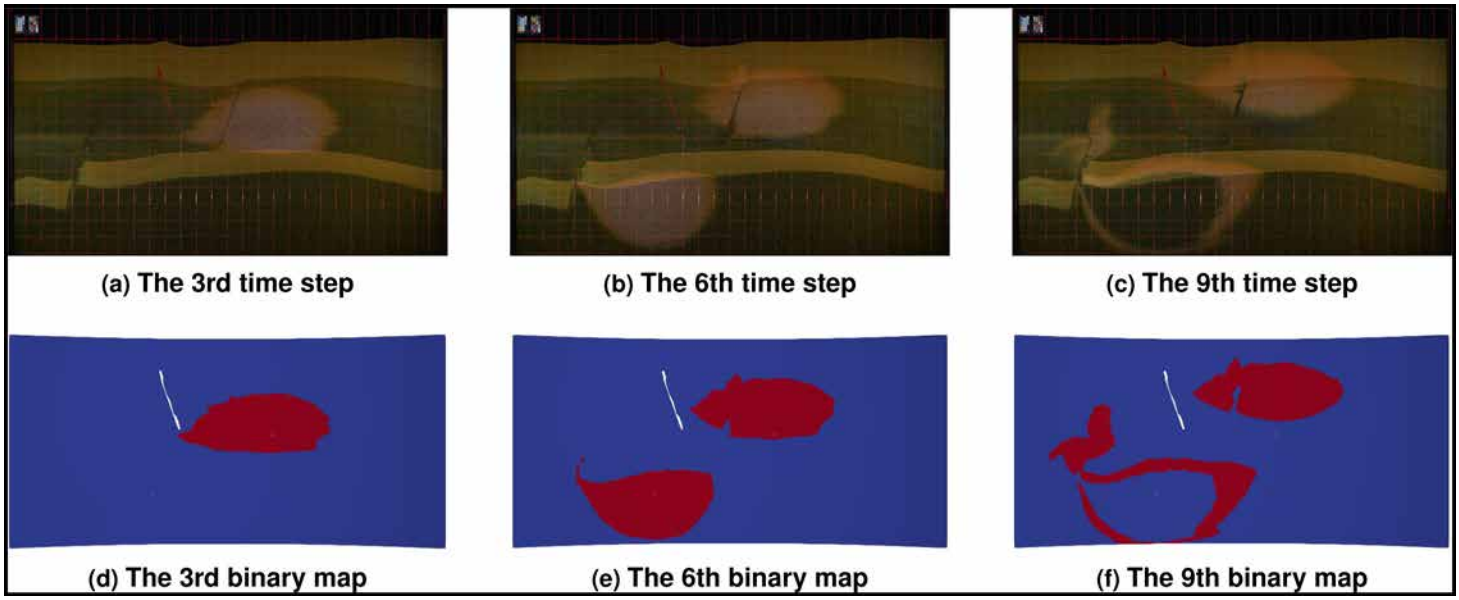

Figure 8—The experimental images of tracer plumes and the associated binary maps. The red region is equal to 1, while the blue region is set to 0

The first row of Figure 8 shows the experimental images of the plume after each stage of tracer injection. The figures in the second row are the associated binary map of the images in the first row. These binary maps will be used as the observations in history matching. However, it is not easy to directly minimize the misfit between the model response and the binary data, as the magnitude and the unit of the model response

are very different from the binary data. Therefore, a hinge loss function is introduced to modify the misfit defined in f_4 of Equation (16). The updated objective function reads:

$$J(u) = H(u)^T H(u) + R(u), \tag{20}$$

where $H(u)$ is the hinge loss function. If the given cell is located at the red region in Figure 8, the hinge loss function is defined as:

$$H(u) = \begin{cases} 0 & \text{if } G(u) > \text{threshold} \\ G(u) - \mathbf{d}_{\text{obs}} & \text{if } G(u) \le \text{threshold} \end{cases}. \tag{21}$$

Note that in this experimental CO_2 storage project, the inverse of the covariance of the measurement error $C_m^{T\,res}$ is not included, as the measurement error is not reported in the experiment description. The threshold is set as 7×10^{-5} in this study. Similarly, when the given cell is located at the blue region in Figure 8, the hinge loss function is defined as:

$$H(u) = \begin{cases} 0 & \text{if } G(u) > \text{threshold} \\ G(u) - \mathbf{d}_{\text{obs}} & \text{if } G(u) \ge \text{threshold} \end{cases}. \tag{22}$$

To consider the uncertainty of the manually filled sand in the experimental rig, the spatial lognormal variations of the permeability are added to the tuned permeability from Table 1. The porosity and the anisotropy of the facies are also included in this table. An example of the tuned permeability field with spatial lognormal variations is shown in Figure 9. The standard deviation of the lognormal variation is set to 0.02. The added variations are spatially correlated using Kriging interpolation and conform to Gaussian variogram model. As it can be seen from the left figure in Figure 9, the layers of the final permeability field contain the spatial variation information from the right figure.

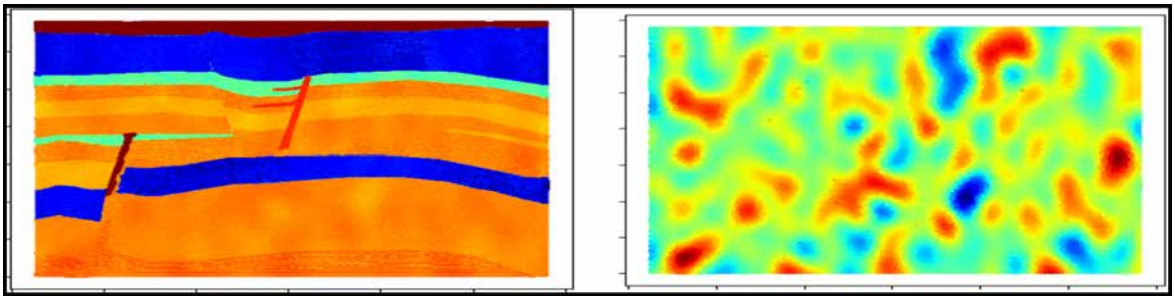

Figure 9—An example of the permeability field with spatial lognormal variation (left) and the corresponding standard normal distribution dataset (right)

Table 1—The tuned petrophysical properties of the facies

Facies	Porosity[-]	Permeability[D]	Anisotropy[x, y, z]
ESF	0.43	34.6	[1, 1,0.316]
C	0.44	302	[1,1,1]
D	0.44	1016	[1,1,1]
E	0.45	549	[1,1,1]
F	0.45	1976	[1,1,1]
G	0.44	1743	[1,1,1]
Fault1	0.44	2554	[1,1,1]
Fault3	0.44	739	[1,1,1]
W	0.44	10 000	[1,1,1]

The generated permeability fields are then taken as the references (i.e. the priors) to train the model to reduce the misfit (i.e. the likelihood) between the model response and observations of binary maps. The history matching results are shown in Figure 10. The tracer plumes of the trained models have a good match with the observations.

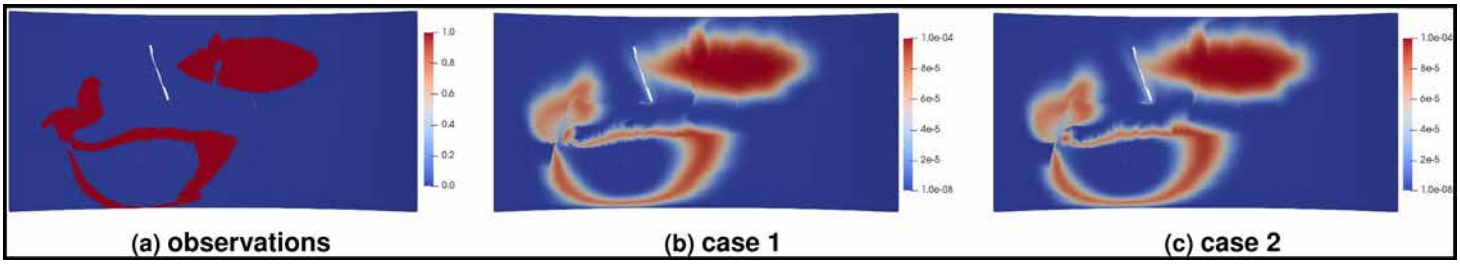

Figure 10—The observations of binary maps and two examples of the history matching results based on the observations. The figures demonstrate the model response of the trained model at the last time step

The computational time of a single evaluation of adjoint gradient for 72262 control variables is around 200 seconds, while the forward simulation takes around 70 seconds. The computation is also executed on the DelftBlue cluster (Delft Blue, 2022) mentioned before. The total computational time of history matching takes around 4 hours.

The associated changes of the permeability after history matching are shown in Figure 11. The plots shown in this figure are calculated by using the permeability after history matching minus the reference permeability (i.e. the prior permeability). There are some zones where the permeability is drastically changed to fit the tracer plumes. Interestingly, these zones are also the regions where the tracer plumes are located. This indicates that the optimizer is able to capture the characteristics of the fluid flow pattern, especially in the regions of plumes where the fluid dynamics are very pronounced.

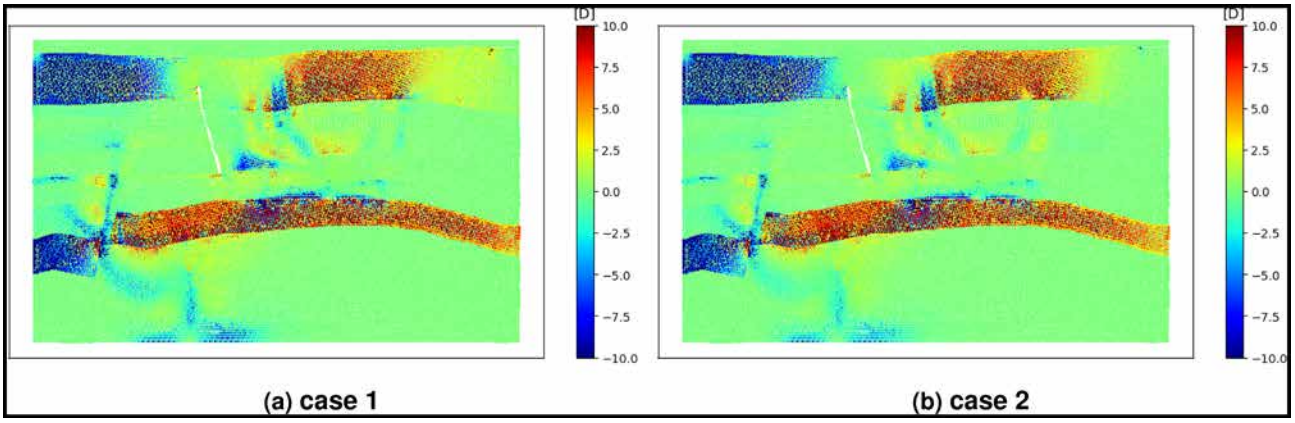

Figure 11—Two examples of the changes of the permeability distribution after the history matching based on the tracer concentration observations

Conclusion

An inverse modeling framework is developed in this study for the applications of the energy transition. This framework is very efficient because of the implementation of the adjoint gradient based on OBL technique. The proposed framework is weakly sensitive to the degrees of freedom of the control variables compared with the conventional numerical gradient method, as the computational time of the adjoint gradient evaluation is comparable to the computational cost of a single forward simulation.

This framework is also designed to allow flexible and various treatments of objective function definitions, for example, well rates, well temperature, BHP, time-lapse reservoir data, and other reservoir data of

interest. The applications of different types of objective function definitions are demonstrated by using three different energy transition examples. A data-driven DiWA model was tested on this framework. For this application, only production data is considered in the objective function. The data diagnostics and multiple attempts of history matching were conducted to achieve good history matching and production forecasting results. In the example of geothermal development, an additional energy balance equation is considered in the governing equations. Accordingly, the time-lapse electromagnetic monitoring data of the geothermal reservoir are added to the objective function to train the model. The results show that electromagnetic monitoring significantly improves the inversion process, as the fluvial channel can be re-constructed to some extent after history matching. The total training time of the geothermal problem with over 70000 control variables is around 8 hours. Similar conclusions can be drawn from the CO_2 storage project in this study. The optimizer is able to capture the characteristics of the fluid flow pattern, especially in the region of plumes where the fluid dynamics are very pronounced. The training time for this project takes around 4 hours. With the feature of adjoint gradient and various types of objective function definitions, this framework allows us to solve the general-purpose inverse modeling problems for most energy transition applications.

Acknowledgements

We would like to thank University of Bergen for the experimental dataset of the CO2 storage FluidFlower project. We also want to thank Oleg Volkov for his suggestions and help with EM inversion.

References

Ahusborde, E., Amaziane, B., and Moulay, M. I. (2021). High performance computing of 3d reactive multiphase flow in porous media: application to geological storage of co2. *Computational Geosciences*, **25** (6):2131 – 2147.

Bukshtynov, V., Volkov, O., Durlofsky, L. J., and Aziz, K. (2015). Comprehensive framework for gradient-based optimization in closed-loop reservoir management. *Computational Geosciences*, **19**(4):877–897.

Datta-Gupta, A. and Datta-Gupta, A. (2007). Streamline Simulation: Theory and Practice. *Society of Petroleum Engineers*, Texas.

Delft Blue (2022). Delft High Performance Computing Centre (DHCP). https://www.tudelft.n1/dhpc/ark:/44463/DelftBluePhasel.

Durlofsky, L. (2005). Upscaling and gridding of fine scale geological models for flow simulation. In *8th International Forum on Reservoir Simulation Iles Borromees*, Stresa, Italy, volume **2024**, pages 1–59.

Evensen, G., Vossepoel, F. C., and van Leeuwen, P. J. (2022). *Data Assimilation Fundamentals*. Springer International Publishing.

Guo, Z., Reynolds, A. C., and Zhao, H. (2018). A physics-based data-driven model for history matching, prediction, and characterization of waterflooding performance. *SPE Journal*, **23**(02):367–395.

Hou, T. Y. and Wu, X.-H. (1997). A multiscale finite element method for elliptic problems in composite materials and porous media. *Journal of Computational Physics*, **134**(1):169–189.

Jansen, J. (2011). Adjoint-based optimization of multi-phase flow through porous media - a review. *Computers and Fluids*, **46** (1): 40–51.

Jansen, J. D., Fonseca, R. M., Kahrobaei, S., Siraj, M. M., Essen, G. M. V., and den Hof, P. M. J. V. (2014). The egg model - a geological ensemble for reservoir simulation. *Geoscience Data Journal*, **1**(2):192–195.

Jenny, P., Lee, S., and Tchelepi, H. (2003). Multi-scale finite-volume method for elliptic problems in subsurface flow simulation. *Journal of Computational Physics*, **187**(1):47–67.

Khait, M. and Voskov, D. (2018a). Adaptive parameterization for solving of thermal/compositional nonlinear flow and transport with buoyancy. *SPE Journal*, **23**(02):522–534.

Khait, M. and Voskov, D. (2018b). Adaptive parameterization for solving of thermal/compositional nonlinear flow and transport with buoyancy. *SPE Journal*, **23**(02):522–534.

Khait, M. and Voskov, D. (2018c). Operator-based linearization for efficient modeling of geothermal processes. *Geothermics*, **74**: 7–18.

Khait, M. and Voskov, D. (2019). Integrated framework for modelling of thermal-compositional multiphase flow in porous media. In *Day 1 Wed*, April 10, 2019. SPE.

Khait, M. and Voskov, D. V. (2017). Operator-based linearization for general purpose reservoir simulation. *Journal of Petroleum Science and Engineering*, **157**:990–998.

Kong, Y., Pang, Z., Shao, H., and Kolditz, O. (2017). Optimization of well-doublet placement in geothermal reservoirs using numerical simulation and economic analysis. *Environmental Earth Sciences*, **76** (3).

Leung, D. Y., Caramanna, G., and Maroto-Valer, M. M. (2014). An overview of current status of carbon dioxide capture and storage technologies. *Renewable and Sustainable Energy Reviews*, **39**:426–443.

Lie, K.-A., Nilsen, H. M., Andersen, O., and Møyner, O. (2015). A simulation workflow for large-scale CO2 storage in the norwegian north sea. *Computational Geosciences*, **20**(3):607–622.

Lyu, X., Voskov, D., and Rossen, W. R. (2021). Numerical investigations of foam-assisted co2 storage in saline aquifers. *International Journal of Greenhouse Gas Control*, **108**:103314.

Stordal, A. S. and Nævdal, G. (2017). A modified randomized maximum likelihood for improved bayesian history matching. *Computational Geosciences*, **22**(1):29–41.

Tian, X., Blinovs, A., Khait, M., and Voskov, D. (2021). Discrete well affinity (DiWA) data-driven proxy model for production forecast. *SPE Journal*, pages 1–17.

Tian, X. and Voskov, D. (2022). Efficient application of stochastic discrete well affinity (DiWA) proxy model with adjoint gradients for production forecast. *Journal of Petroleum Science and Engineering*, **210**:109911.

Vo, H. X. and Durlofsky, L. J. (2014). A new differentiable parameterization based on principal component analysis for the low-dimensional representation of complex geological models. *Mathematical Geosciences*, **46**(7):775–813.

Volkov, O. and Voskov, D. (2016). Effect of time stepping strategy on adjoint-based production optimization. *Computational Geosciences*, **20** (3):707 – 722.

Voskov, D. (2017a). Operator-based linearization approach for modeling of multiphase multi-component flow in porous media. *Journal of Computational Physics*, **337**:275–288.

Voskov, D. V. (2017b). Operator-based linearization approach for modeling of multiphase multi-component flow in porous media. *Journal of Computational Physics*, **337**:275–288.

Voskov, D. V., Henley, H., and Lucia, A. (2017). Fully compositional multi-scale reservoir simulation of various CO2 sequestration mechanisms. *Computers & Chemical Engineering*, **96**:183–195.

Wang, Y., Voskov, D., Khait, M., and Bruhn, D. (2020). An efficient numerical simulator for geothermal simulation: Abenchmark study. *Applied Energy*, **264**.

Wapperom, M., Lyu, X., and Voskov, D. (2022). Accurate modeling of near-wellbore effects induced by supercritical CO2 injection. In *ECMOR 2022*. European Association of Geoscientists & Engineers.

Zaydullin, R., Voskov, D., and Tchelepi, H. (2013). Formulation and solution of compositional displacements in tie-simplex space. In *SPE Reservoir Simulation Symposium*. *Society of Petroleum Engineers*.

Zaydullin, R., Voskov, D., and Tchelepi, H. A. (2012). Nonlinear formulation based on an equation-of-state free method for compositional flow simulation. *SPE Journal*, **18**(02):264–273.